Synthesis and characterization of vacancy-doped neodymium telluride for thermoelectric applications

Steven J. Gomez,[1,2†] Dean Cheikh,[1†] Trinh Vo,[1] Paul Von Allmen,[1] Kathleen Lee,[1] Max Wood,[3] G. Jeff Snyder,[3] Bruce S. Dunn,[2] Jean-Pierre Fleurial,[1] and Sabah K. Bux[1*]

[1]Thermal Energy Conversion Technologies Research and Advancement Group, Jet Propulsion Laboratory, California Institute of Technology, 4800 Oak Grove Drive, Pasadena, California 91109-8099

[2]Department of Materials Science and Engineering, University of California, Los Angeles 90092

[3]Department of Materials Science and Engineering, Northwestern University, Evanston, Illinois 60208

[†]These authors contributed equally to this work.

Supplemental Data

Table S1: Sample porosities listed along with theoretical and measured densities of pressed $Nd_{3-x}Te_4$ samples. Theoretical densities were predicted using nominal compositions. Measurements were performed using the Archimedes method, showing densities above 96% of theoretical values. The nominal $Nd_{2.72}Te_4$ sample shows a high amount of porosity (5%) mainly from pullout during polishing, a result of the sample being mechanically weak.

Nominal Composition	Theoretical Density (g cm^{-3})	Measured Density (g cm^{-3})	Calculated Porosity
Nd_3Te_4	7.46	7.17	0.12%
$Nd_{2.90}Te_4$	7.34	7.27	0.086%
$Nd_{2.86}Te_4$	7.30	7.24	0.023%
$Nd_{2.79}Te_4$	7.23	7.22	0.033%
$Nd_{2.74}Te_4$	7.16	7.12	0.068%
$Nd_{2.72}Te_4$	7.14	7.08	4.977%

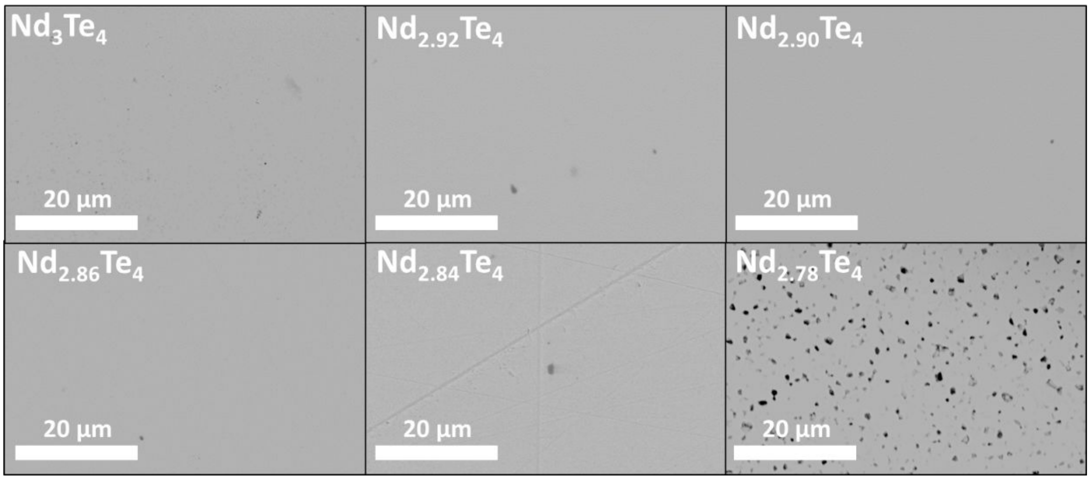

Figure S1: BSE SEM images (5000x) of $Nd_{3-x}Te_4$ at various vacancy concentrations. The uniformity of the image contrast reflects the homogeneity of the samples. Dark areas are indicative of sample porosity. Sample porosities for all samples except $Nd_{2.78}Te_4$ were less than 0.1%, calculated using an area fraction of each SEM image. The $Nd_{2.78}Te_4$ sample shows a high amount of porosity (5%) mainly from pullout during polishing, a result of the sample being mechanically weak.

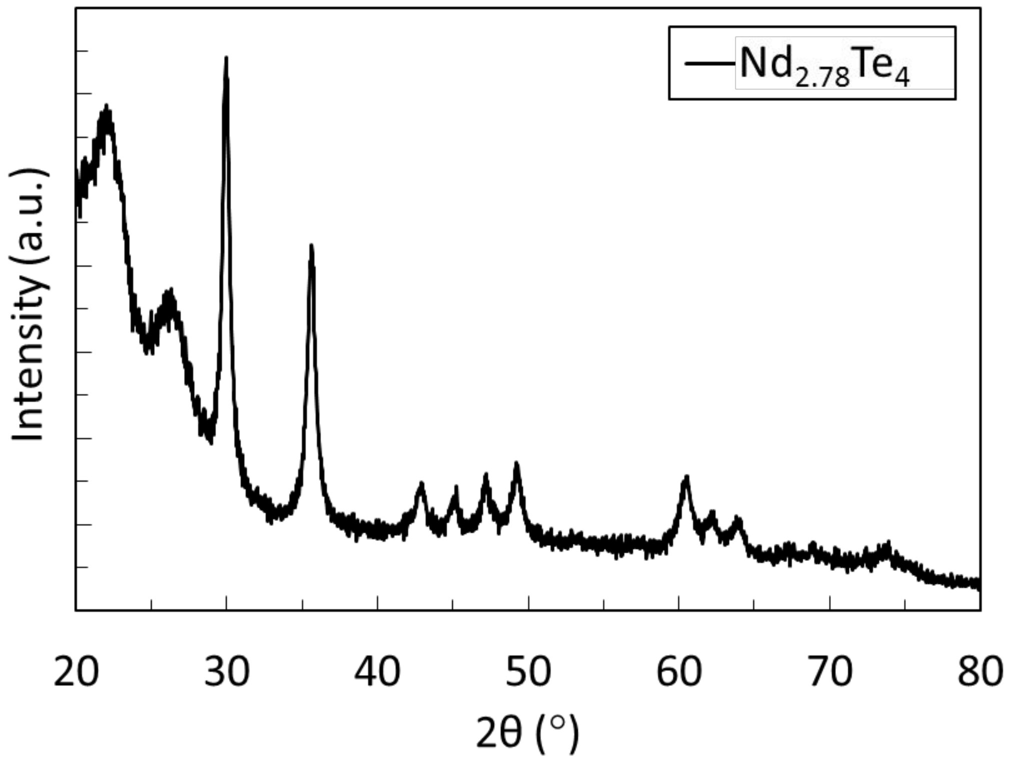

Figure S2: X-ray diffraction patterns for $Nd_{3-x}Te_4$ powder immediately after ball milling, confirming the Th_3P_4 structure type. Significant background for values of 2θ below 30° is caused by a Kapton film in the sample holder.

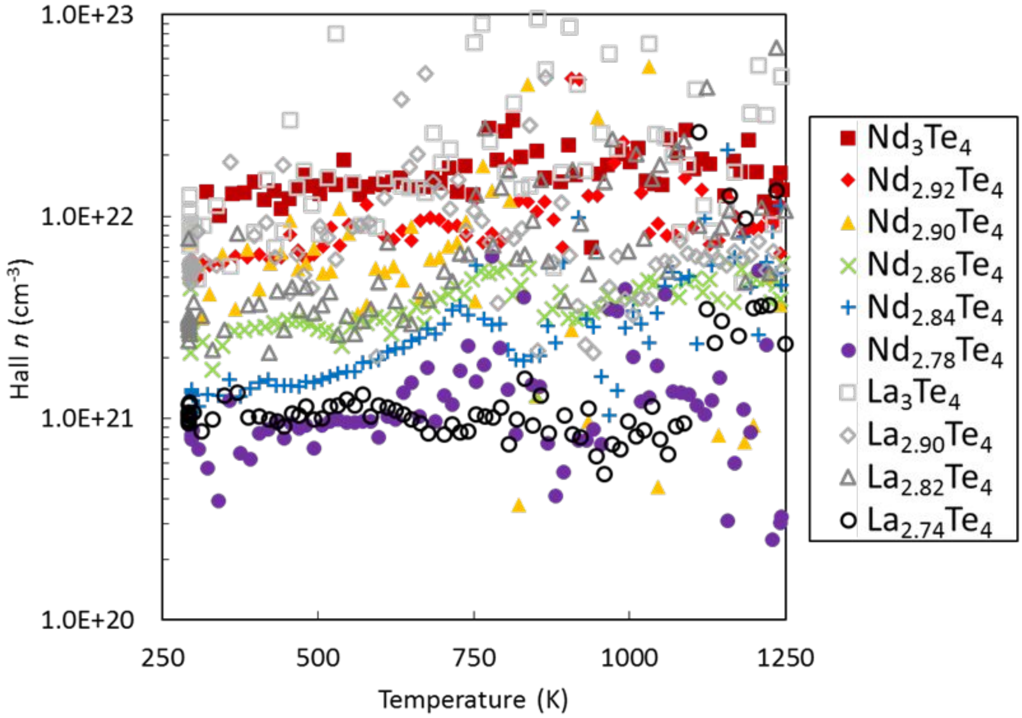

Figure S3: Temperature-dependent carrier concentration for $Nd_{3-x}Te_4$ samples compared to $La_{3-x}Te_4$.

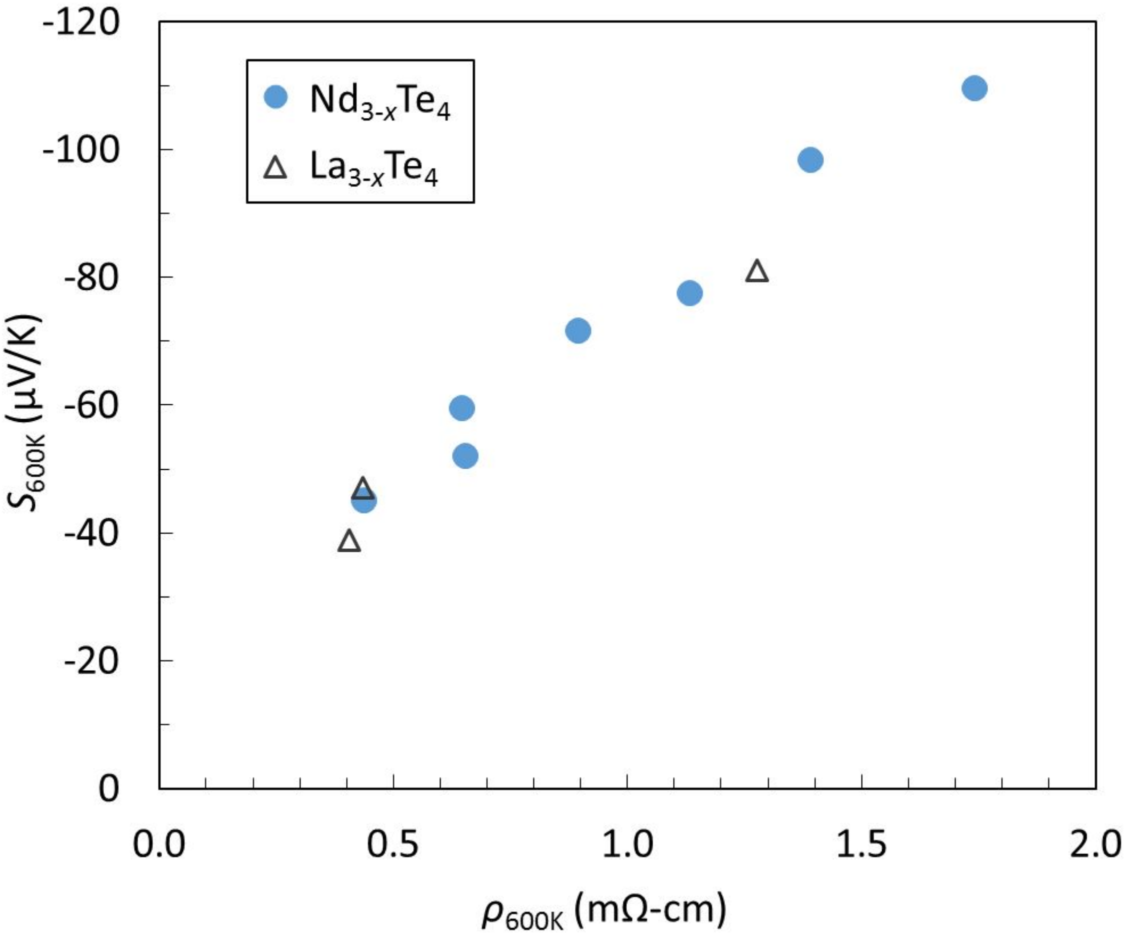

Figure S4: Plot of Seebeck vs. resistivity at 600 K for $Nd_{3-x}Te_4$ and $La_{3-x}Te_4$.[10] The simultaneous increase in Seebeck and resistivity agrees with the decrease in carrier concentration.

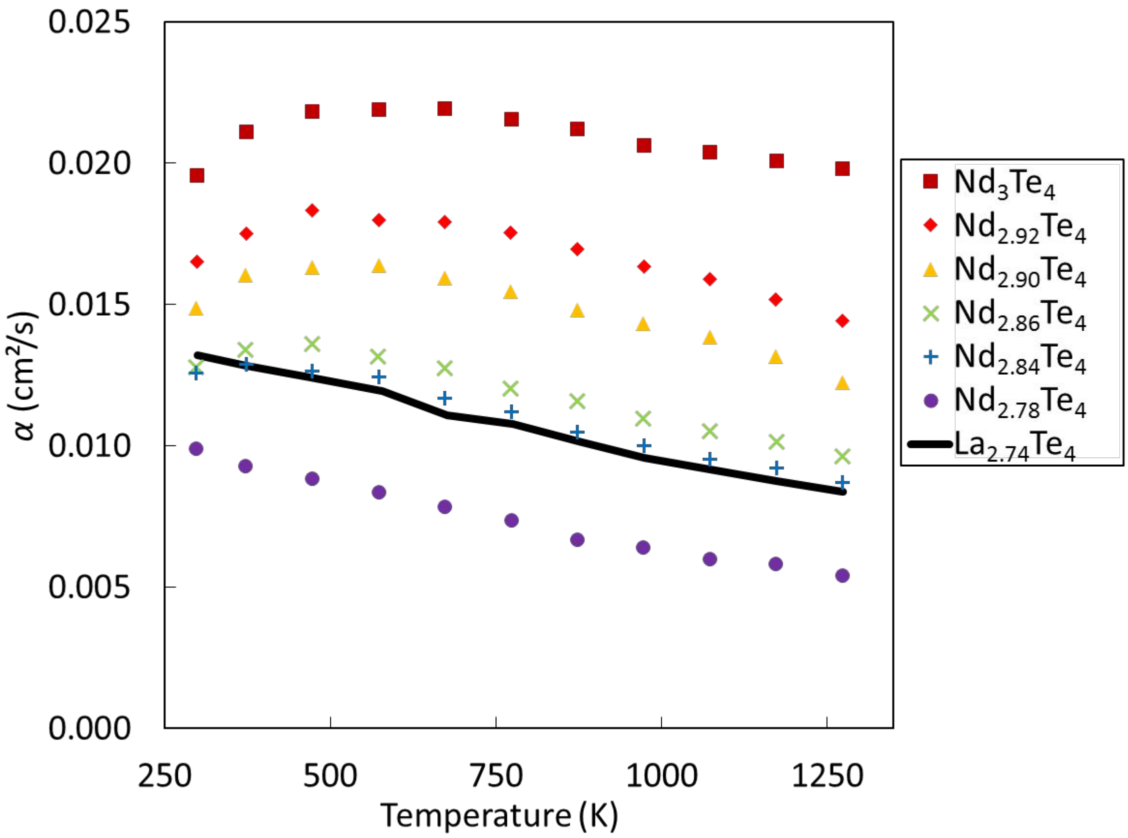

Figure S5: Temperature dependent thermal diffusivity of $Nd_{3-x}Te_4$ compared to that of $La_{2.74}Te_4$.

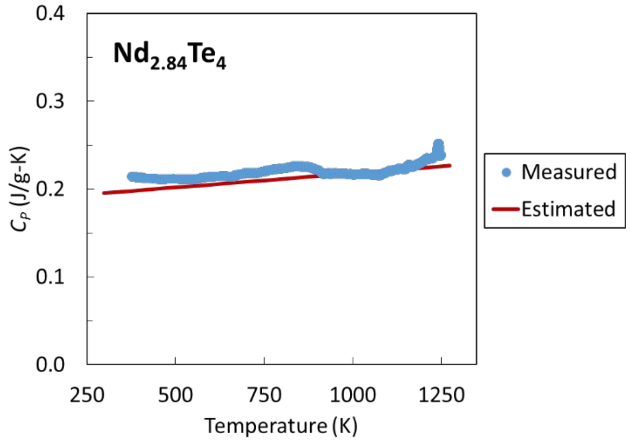

Figure S6: Measured temperature dependent heat capacity for $Nd_{2.84}Te_4$, compared against values estimated by multiplying the heat capacity of La_3Te_4 by the ratio of the molecular weights. Both samples show excellent agreement between estimated and measured values.

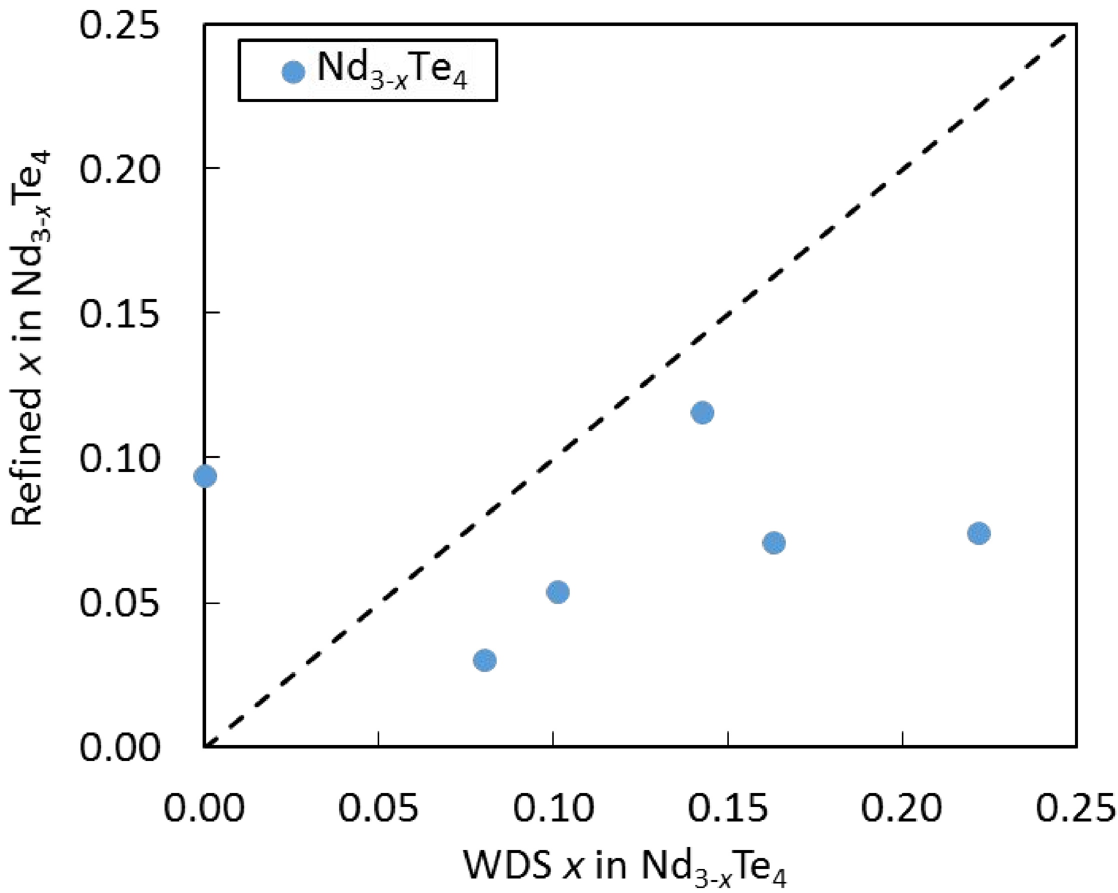

Figure S7: Refined x in $Nd_{3-x}Te_4$ obtained by Rietveld refinement versus measured x obtained by WDS.

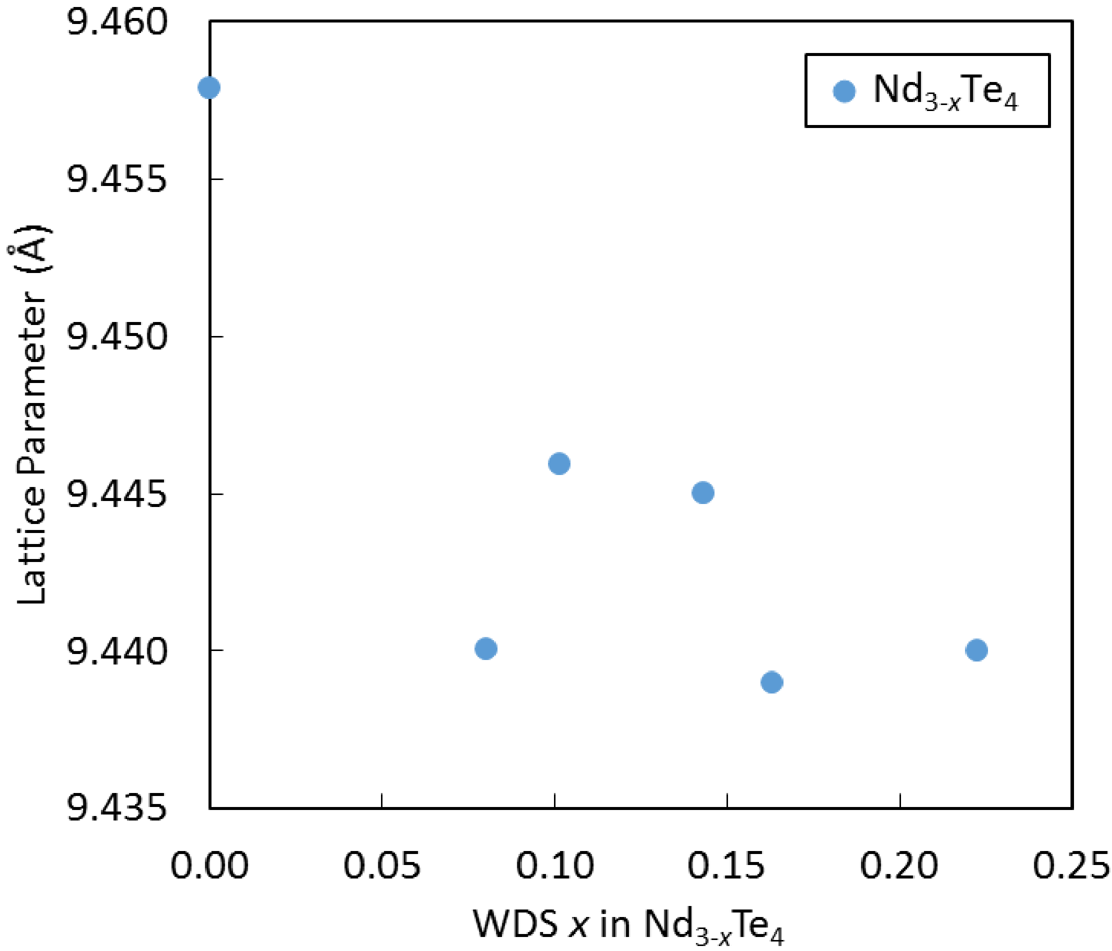

Figure S10: Refined lattice parameter obtained by Rietveld refinement as a function of measured x in $Nd_{3-x}Te_4$ obtained by WDS. These are in good agreement with the published value of 9.435 Å.[26]

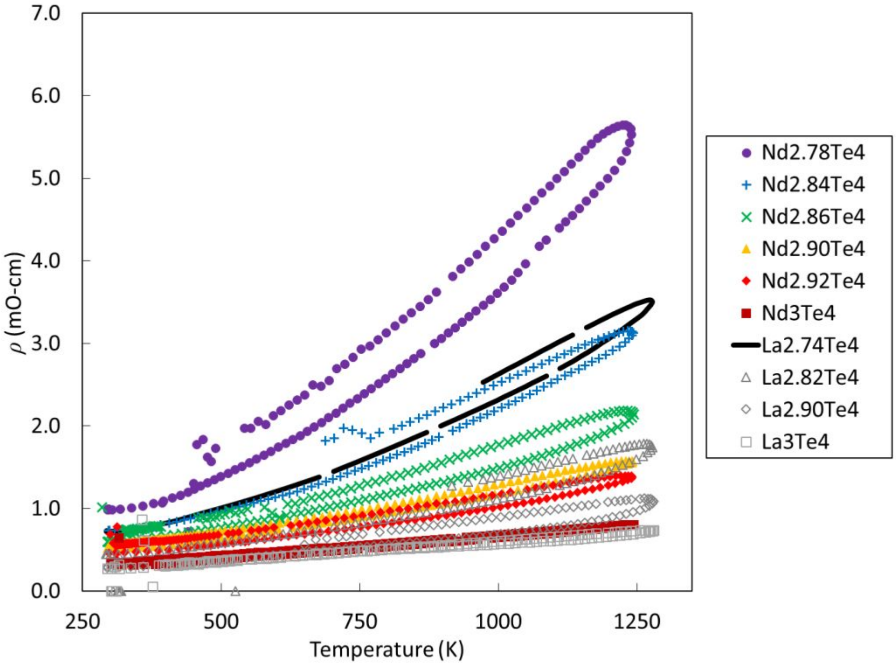

Figure S11: Heating and cooling cycles for temperature-dependent resistivity measurements showing only small hysteresis.

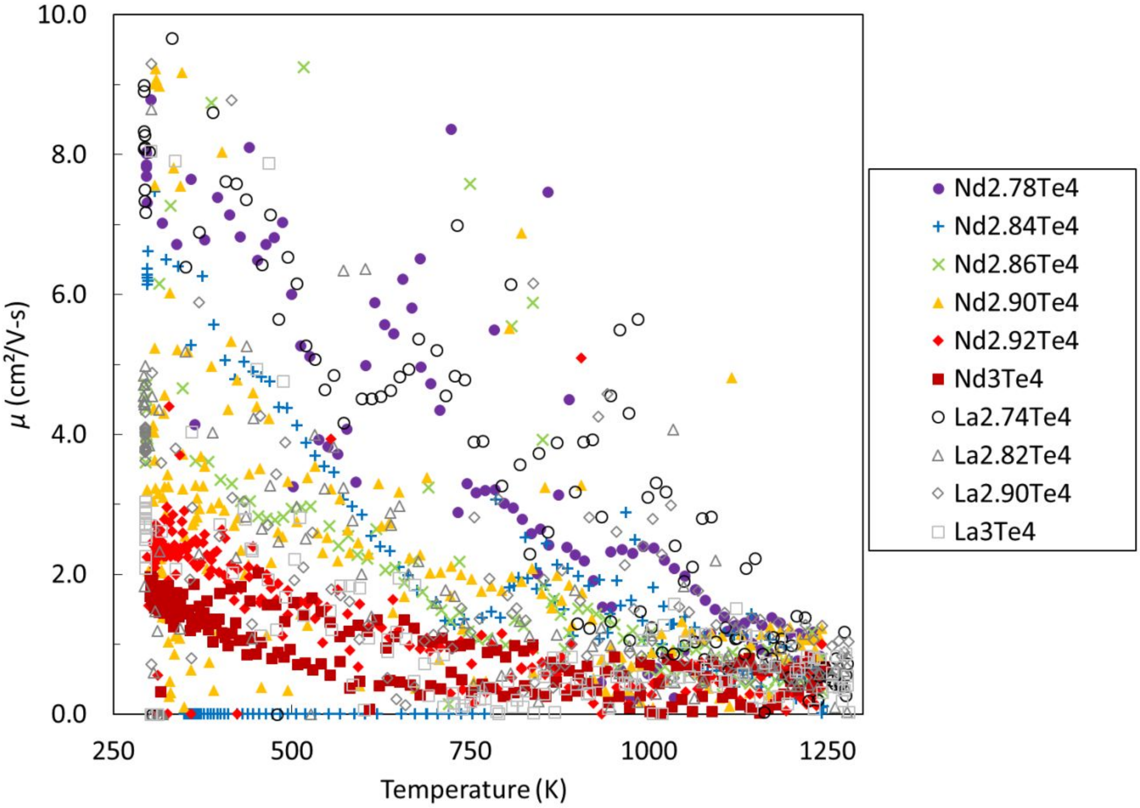

Figure S12: Heating and cooling cycles for temperature-dependent mobility measurements.

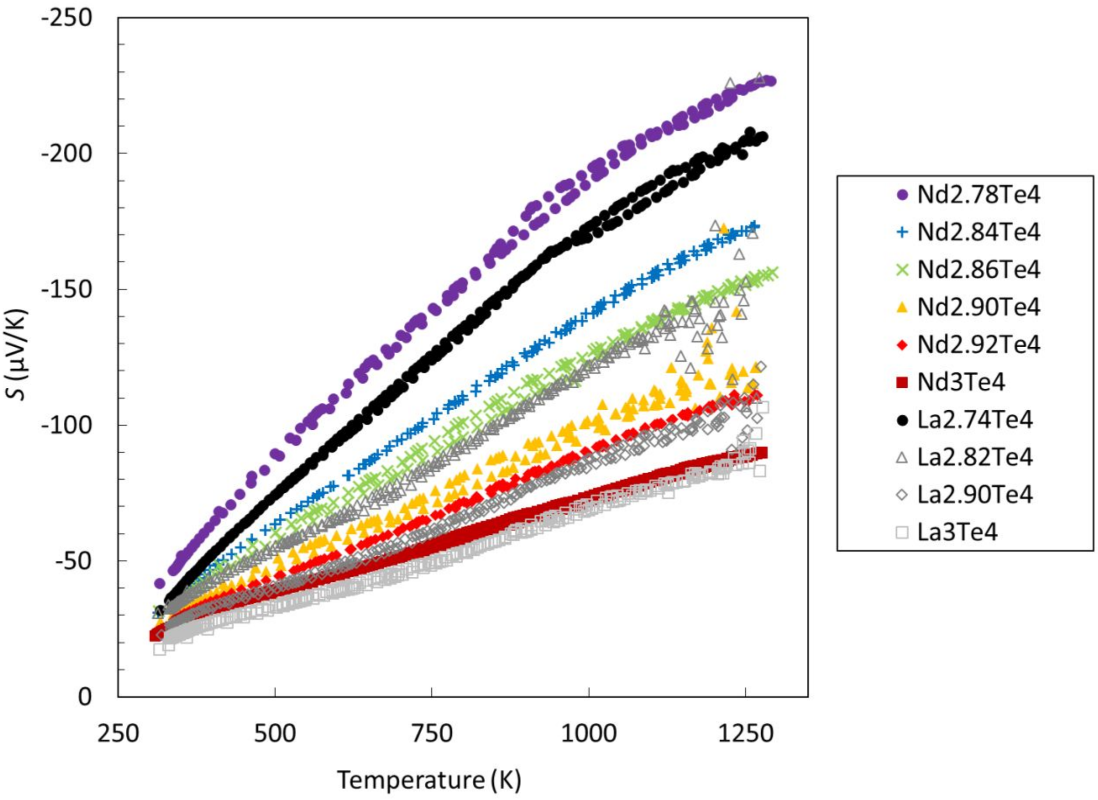

Figure S13: Heating and cooling cycles for temperature-dependent Seebeck coefficient measurements showing excellent agreement between heating and cooling data.